Journal of Physics: Conference Series

A test of the v^2-f k- turbulence model for the prediction of vortex shedding in the Francis-99 hydrofoil test case

IOP Conf. Series: Journal of Physics: Conf. Series **1296** (2019) 012004 doi:10.1088/1742-6596/1296/1/012004

A test of the v^2-f k-ϵ turbulence model for the prediction of vortex shedding in the Francis-99 hydrofoil test case

K F Sagmo[1], P T Storli[1]

[1] Waterpower Laboratory, Norwegian University of Science and Technology, Alfred Getz Vei 4, 7491 Trondheim, Norway

E-mail: kristian.sagmo@ntnu.no

Abstract. A test of the $v^2 - f$ $k - \epsilon$ turbulence model for the flow around the Francis-99 hydrofoil geometry is conducted in order to assess it's accuracy of trailing edge vortex shedding prediction. The model is based on the $k - \epsilon$ turbulence model, but needs no wall damping function, and also allows near-wall turbulence anisotropy. For reference, the model results are compared with the the SST $k - \omega$, in addition to preliminary experimental results previously published. It is indicated that the $v^2 - f$ $k - \epsilon$ model gives at least as good, or better results than the more commonly used SST $k - \omega$ model for the present case, though further measurements are needed in order to make a proper conclusion.

1. Introduction

One step towards an accurate fluid structure interaction (FSI) simulation is an accurate modeling of the computational fluid dynamics (CFD) domain. Typically, eddy resolving simulations are considered too expensive for an FSI simulation, so instead a Reynolds Averaged Navier stokes (RANS) approach with an accurate turbulence closure model is sought. For the present case in particular, accurate prediction of separation is important. The $v^2 - f$ $k - \epsilon$ turbulence model has previously proven effective for such problems[1, 2]. The model allows for near wall turbulence anisotropy, by setting the appropriate boundary condition for the elliptic function f near a wall, ensuring that the velocity scalar $\overline{v^2}$ behaves like the wall normal Reynolds stress component as the wall normal distance goes to zero. The benefit of the model's ability to capture the suppression of the normal component of the turbulence near a wall relative to the tangential components eliminates the need to dampen the modeled eddy viscosity in this region. This is demonstrated by excellent agreement of the model near wall eddy viscosity compared with DNS data for the eddy viscosity in channel flow[3].

2. Methods

2.1. Computational domain and boundary conditions

The numerical simulations were carried out on a trimmed, semi-regular hexahedral 3D grid, set up in accordance with the experimental geometry to allow for direct comparison of the results. No-slip conditions were specified at all walls, and y^+ values were kept below 1 in order to resolve the sub-viscous boundary layer and avoid the use of wall functions. A cross section

view of the computational domain and grid, along with the position of the velocity inlet and the environmentally specified atmospheric pressure outlet is presented in figure 1. Also defined is the foil trailing edge thickness $D = 4.8$ mm, and the foil chord length $c = 250$ mm. All simulations were carried out at a test section bulk velocity of 9.1 m/s, or a Reynolds number of about $2.3 \cdot 10^6$, matching the experimental conditions described by Sagmo et. al[4] and Bergan et. al[5]. The hydrofoil goes through vortex induced resonance at bulk velocities of around 11.6 m/s, which is deemed sufficiently far away for a purely computational fluid dynamics simulation to be accurate at the present test section inflow conditions.

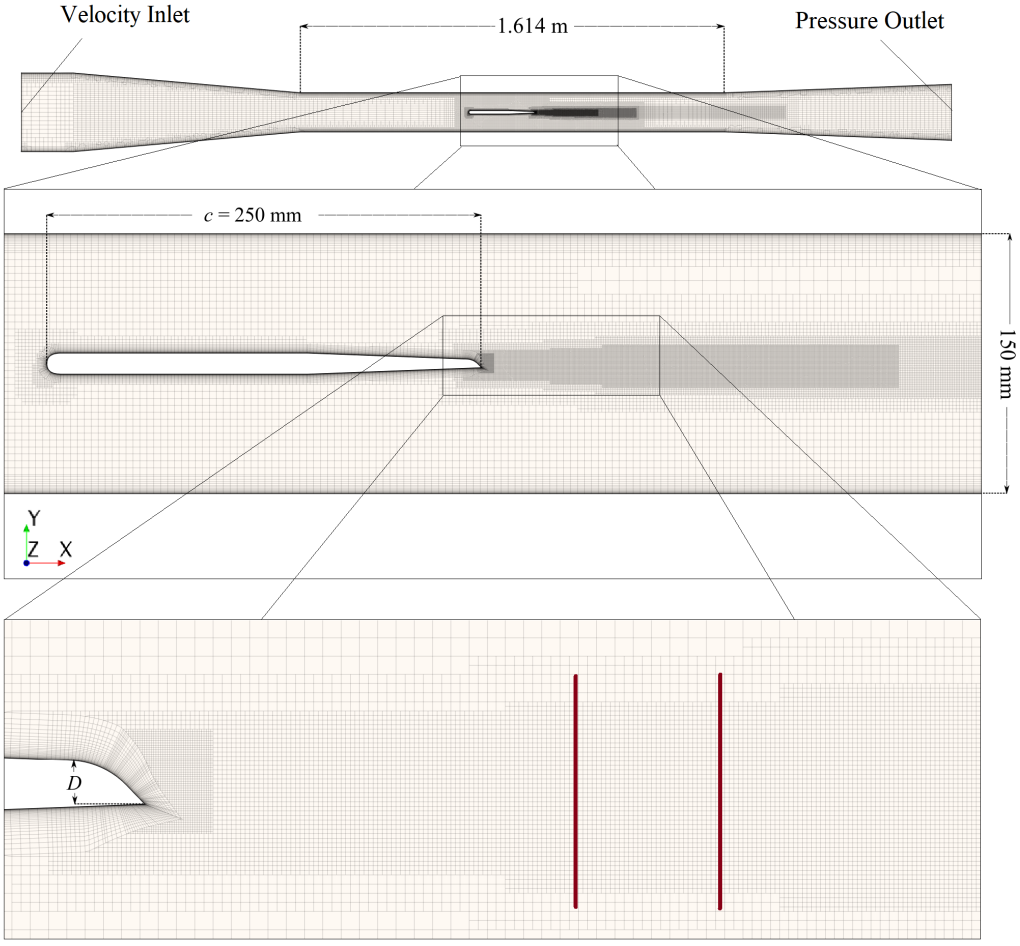

Figure 1: Mid section of computational domain grid in successively enlarged views. The orientation of the coordinate system is also indicated. The two bold red vertical lines in the bottom enlargement from left to right indicates the velocity sampling positions at X=9.9D and X=13.3D downstream of the trailing edge tip, respectively.

In the experimental test rig, the straight circular pipe leading into the test section, seen in the top view of figure 1, extends about 21 diameters upstream before encountering a 90 degree bend with stationary vanes. As such, the incoming pipe flow is assumed to be nearly fully developed, though measurements are needed in order to confirm this. During setup of the simulations several positions of the velocity inlet was tested with steady state RANS calculations, in order to check the sensitivity of the test section velocity profile as a function of the incoming pipe velocity profile. Figure 2 give the results for three different inlet positions; A - at the beginning of

the quadratic test section, B - the inlet position shown in figure 1 and C - a further 6 m upstream of position B. It was found that a flow development length of about 20 diameters upstream of the convergent section lead to a slightly more developed test section velocity profile with a center line velocity increase of roughly 2 % (evaluated about $1.5c$ upstream of the hydrofoil) compared to a uniform velocity profile set at the start of the test section. The near fully developed pipe velocity profile extracted from inlet position C was therefore specified at the velocity inlet shown in figure 1 for the simulations later presented. The location of the pressure outlet was also varied to ensure that the positioning had negligible impact on the simulation results.

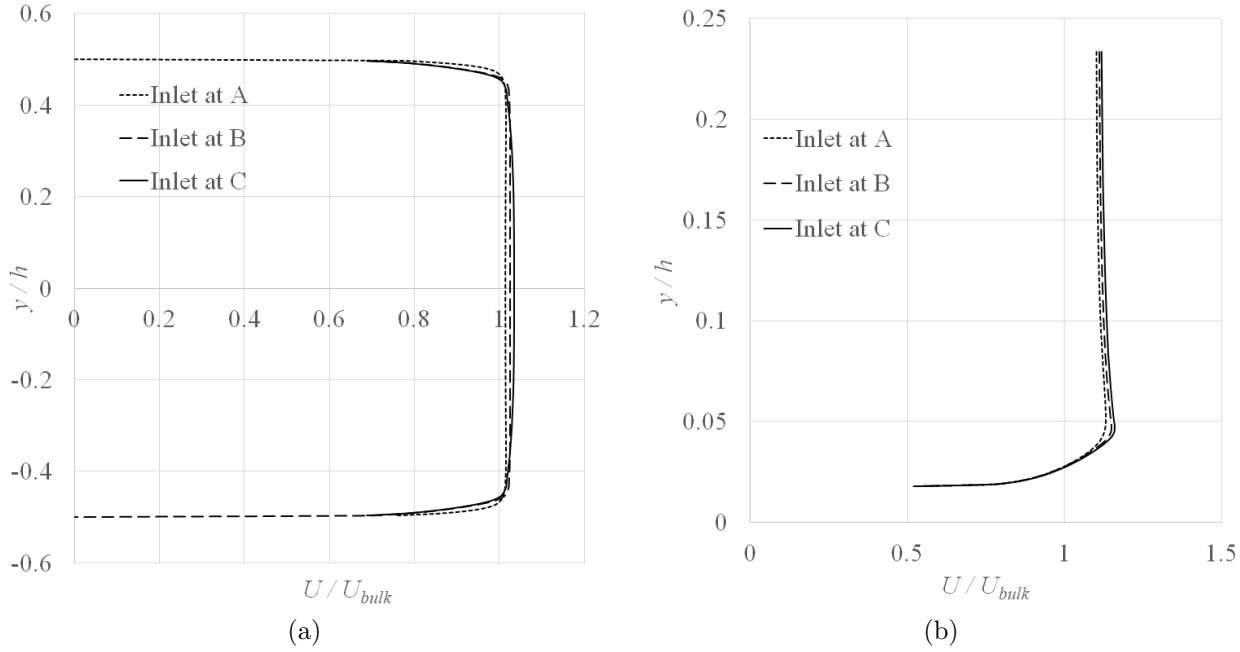

Figure 2: Effects of moving the velocity inlet upstream from position A to B and C. (a) Resulting test section velocity-profile approximately $1.5c$ upstream. (b) Resulting trailing edge velocity profiles at X=$0.96c$

A uniform turbulence intensity, TI of 5% was specified at the inlet, along with a turbulent length scale, L, of 1/6 times the pipe radius of 150 mm. The necessary model turbulence parameters, the turbulent kinetic energy k, the turbulent dissipation rate ϵ, the velocity scalar $\overline{v^2}$ and the specific dissipation rate ω, were then derived by the relations[6]:

$$k = \frac{3}{2}(TI|\mathbf{u}|)^2, \quad \epsilon = C_\mu \frac{k^{3/2}}{L}, \quad \overline{v^2} = \frac{2}{3}k, \quad \omega = \beta^{*-1/4}\frac{\sqrt{k}}{L}. \tag{1}$$

Above, $|\mathbf{u}|$ denotes the local velocity magnitude, and C_μ as well as β^* are model coefficients.

Unfortunately, experimental values for the turbulence intensity and turbulent length scale are not yet available for the test section. In order to give some indication of the sensitivity of the model results on the turbulence intensity, another set of simulations were conducted with a 20% inlet TI. To give some indication of the modeled decay of the turbulence table 1 shows the specified turbulence intensities at the inlet, along with corresponding turbulence intensities both upstream of the hydrofoil and at the trailing edge, just outside the boundary layer.

2.2. Turbulence models and solvers

The present work focuses on the v^2-f k-ϵ turbulence model, with the model transport equations as described by Durbin[2] as well as Parneix et al.[7].

Table 1: Turbulence intensity levels (TI) at different stream-wise positions in the computational domain, relative to the hydrofoil leading edge (X=0).

Inlet	X=-1.5c	X=0.95c
5%	1.8%	1.2%
20%	4.7%	3%

The second turbulence model utilised, for reference, is the widely used Shear Stress Transport (SST) k-ω turbulence model, presented by Menter[8]. In addition, in order to investigate the effect of laminar to turbulent transition on the case, the Langtry-Menter γ-Re$_\theta$ transition model[9] was run with the SST k-ω turbulence model. This model put the strictest constraints on the design of the mesh, such as limiting the wall cell layer thickness growth rate to 1.2, preferably 1.1, according to recommended practice[10]. This resulted in a wall cell layer growth rate of 1.15 over the hydrofoil surface. The γ-Re$_\theta$ transition model requires the definition of a free stream function. For simplicity, and from inspection of preliminary results with the steady state RANS simulations this function was specified as a step function going from zero to unity outside a 8 mm wall distance. The model coefficients as implemented in Star-CCM+ are described in the paper by Malan et al.[11]

All models were run with a segregated velocity-pressure correction solver, according to the SIMPLE algorithm. For comparability, the upwind flow convection scheme was set to second order, as was the solvers for the turbulence equations. All turbulence models constitutive relations were linear, i.e. according to the classic Boussinesq approximation. Further, a realizability constraint was set for both models, according to Durbin's scale limiter presented in [12].

2.3. Sampling periods and temporal discretization

The transient simulations were initiated from steady state solutions converged to normalized residuals of order 10^{-4} or less of all transported variables. For each successive time step, 6 inner iterations were run, which again ensured that all normalized residuals had reached values of order 10^{-4} or less. All simulations were run approximately 50 trailing edge vortex shedding periods before sampling of mean quantities were initiated and run for a successive 100 shedding periods.

An implicit temporal solver of 2'nd order was used and the time-step was set to $2.5 \cdot 10^{-5}$ s, such that the convective Courant number, C_n, achieved was around 1 in the wake of the trailing edge, and less than 2 for the vast majority of the computational domain. This further ensured around 80 time-steps per shedding period. For the coarse and fine grids used in the calculation of the grid discretization error the time-steps were adjusted in order to keep the C_n comparable for all 3 grids.

The trailing edge shedding frequency Strouhal number, St, was computed using Welch's method to obtain the power spectra of the cross stream velocity fluctuations sampled in the wake. The mean stream-wise velocity was sampled at positions indicated in figure 1.

2.4. Discretization error estimation and iterative errors

The grid convergence index, GCI was calculated by the procedure recommended by Celik et. al.[13]. The simulations with the v^2-f k-ϵ turbulence model were run at 3 different grids, with a refinement rate of roughly 1.5 in between each grid. The results from the grid refinement study are presented in the next section.

Further, temporal iterative errors were investigated for all simulations by checking results

at sampling periods corresponding to roughly 50 and 100 shedding periods, showing negligible differences compared to the differences in the solutions on the different grids.

3. Results

3.1. Grid discretization error estimates

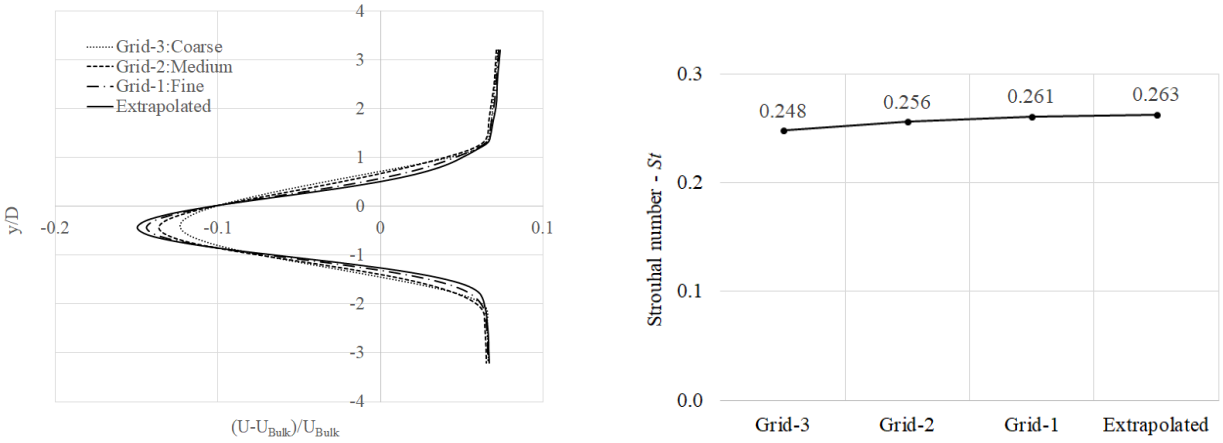

(a) (b)

Figure 3: Solutions for different grids with the v^2-f model (a) Wake profiles for X=9.9D (b) Strouhal numbers based on bulk velocity and D.

Figure 3 illustrates the grid dependency for the both the velocity profile at 9.9D and the obtained Strouhal numbers for the present Reynolds number of $2.3 \cdot 10^6$. The cell count for each grid, going from coarse to fine were; $11.66 \cdot 10^6, 20.88 \cdot 10^6$ and $52.05 \cdot 10^6$. Results are for the v^2-f k-ϵ turbulence model. All results given below are with the medium grid, due to the computational expense of having to run all turbulence models on the fine grid, for comparison. From the wake profiles, an average observed numerical order, p_{obs}=1.9 was calculated. This was used to calculate the GCI plotted with the below results for the velocity profiles. From the obtained Strouhal numbers, a p_{obs}=2.7 was calculated, and subsequently used for the GCI plotted with the Strouhal numbers in figure 5. Seen in conjunction, the calculated numerical orders are in good agreement with the selected 2'nd order numerical schemes.

3.2. Comparison of Models and Measurement

Figure 4 presents the simulated wake profiles at the two locations indicated in figure 1. Finally figure 5 compares the obtained Strouhal numbers from all models.

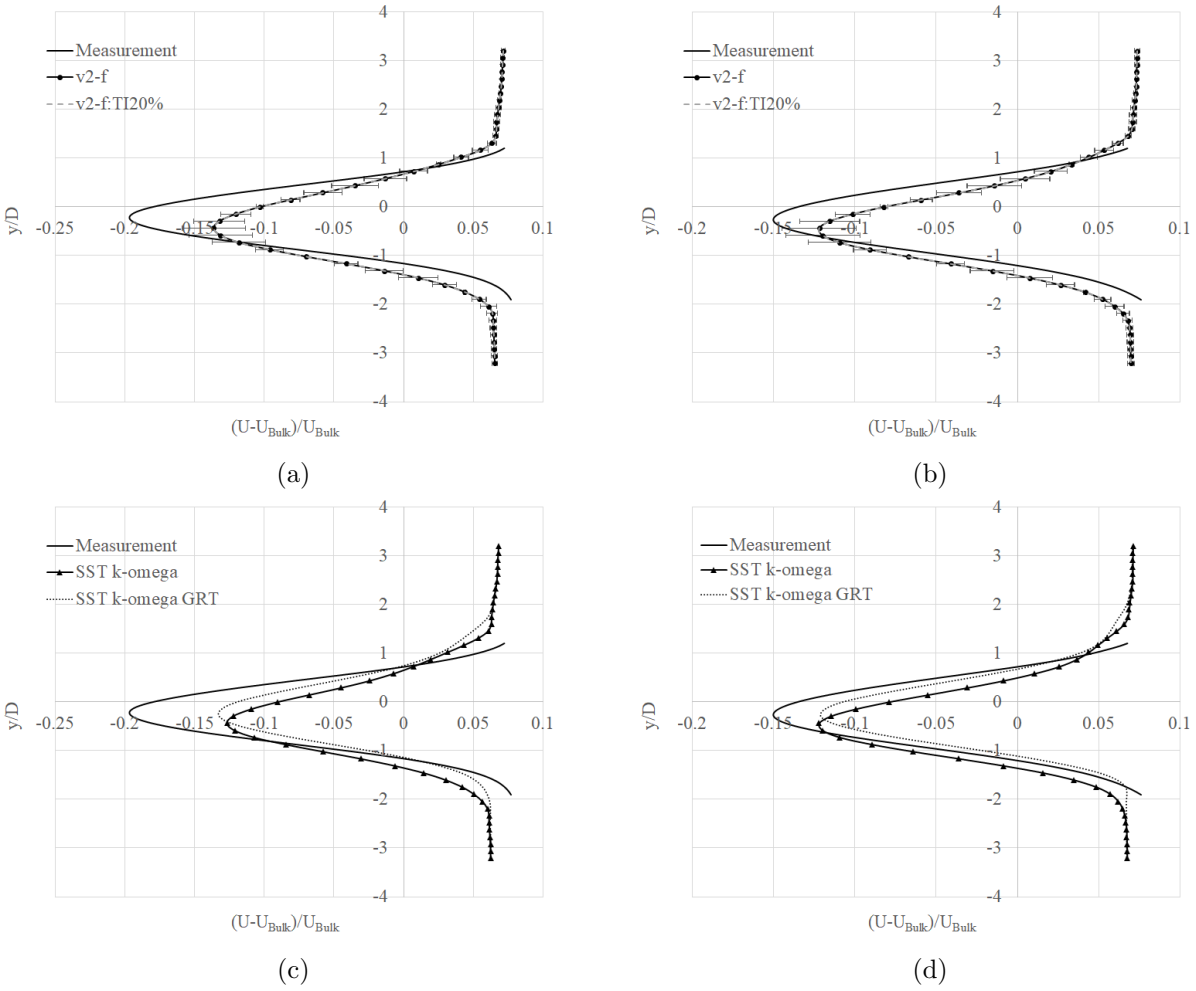

Figure 4: Velocity profiles downstream of the trailing edge for different models compared to experiment. In the left column (a and c) sampled at X=9.9D. In the right column (b and d) sampled at X=13.3D. The error bars represent one GCI to each direction.

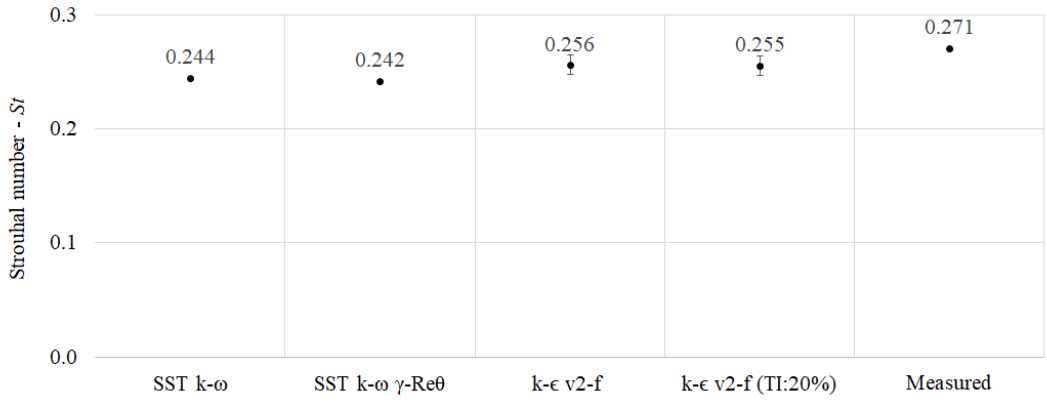

Figure 5: Strouhal numbers obtained for all models on the medium grid.

4. Discussion and Conclusion

In figure 4 a and b the small variation in the free stream TI close to the trailing edge of 3% compared to 1.2%, obtained from specifying a high turbulence inlet value of 20%, is seen to have negligible impact on the wake profile at both downstream positions. Still, it may well be that a larger TI variation, hitting some critical value could give substantially different results. In addition, transition from laminar to turbulent flow modeled with the γ-Re$_\theta$ formulation is seen to have little impact on the wake profiles. Though not shown, this is due to the model predicting transition quite close to the leading edge, at about X=0.03c.

Overall the v^2-f model again agrees somewhat better with experimental values than the other models. It is assumed that a slightly better prediction of the upper separation point is the root cause of this, though experiments are needed to confirm this. It is noted a small variation in the free stream turbulence intensity, has only a negligible effect on the velocity profile downstream of the trailing edge, though without a proper assessment of the test section turbulence levels and upstream velocity profile, this may still be incidental. Nevertheless, considering the sensitivity tests carried out with respect to the free stream turbulence intensity and transition, the results indicate that the v^2-f model does give at least as good results, or better, compared to the SST k-ω turbulence model for the present test case.

Acknowledgments

This work was supported with computational resources provided by UNINETT Sigma2. The measurement work previously presented was made with support from the HiFrancis project.

References

[1] Iaccarino G 2001 *Journal of Fluids Engineering* **123** 819 ISSN 00982202 URL http://FluidsEngineering.asmedigitalcollection.asme.org/article.aspx?articleid=1484326
[2] Durbin P A 1995 *AIAA Journal* **33** 659–664 ISSN 0001-1452, 1533-385X URL http://arc.aiaa.org/doi/10.2514/3.12628
[3] Durbin P A and Reif B A P 2011 *Statistical Theory and Modeling for Turbulent Flows* 2nd ed (West Sussex, United Kingdom: John Wiley Sons) ISBN 978-0-470-68931-8
[4] Sagmo K F, Tengs E O, Bergan C W and Storli P T 2019 *IOP Conference Series: Earth and Environmental Science* **240** 062006 URL
[5] Bergan C, Solemslie B, Østby P and Dahlhaug O G 2018 *International Journal of Fluid Machinery and Systems* Accepted
[6] Siemens/CD-Adapco *StarCCM+ user guide* code version 12.02.010
[7] Parneix S, Durbin P A and Behnia M *Flow, Turbulence and Combustion* **60** 19–46
[8] Menter F R 1994 *AIAA journal* **32** 1598–1605
[9] Langtry R B and Menter F R 2009 *AIAA Journal* **47** 2894–2906
[10] Langtry R B 2006 *A Correlation-Based Transition Model using Local Variables for Unstructured Parallelized CFD codes* Ph.D. thesis University of Stuttgart
[11] Malan P, Suluksna K and Juntasaro E 2009 *the 47th AIAA Aerospaces Sciences Meeting*
[12] Durbin P 1996 *International Journal of Heat and Fluid Flow* **17** 89–90 ISSN 0142727X URL http://linkinghub.elsevier.com/retrieve/pii/0142727X9500073Y
[13] Celik I B, Ghia U, Roache P J, Freitas C J, Coleman H and Raad P E 2008 *Journal of Fluids Engineering* **130** 078001–078001–4 ISSN 0098-2202 URL http://dx.doi.org/10.1115/1.2960953